China Ocean Eng., Vol. 26, No. 2, pp. 185 − 194

DOI 10.1007/s 10.1007/s13344-012-0014-4 ISSN 0890-5487

A Numerical Model for Ultimate Soil Resistance to An Untrenched Pipeline Under Ocean Currents*

GAO Fu-ping (高福平)[1], HAN Xi-ting (韩希霆) and YAN Shu-ming (闫术明)

Institute of Mechanics, *Chinese Academy of Sciences*, *Beijing 100190*, *China*

(Received 31 October 2011; received revised form 26 December 2011; accepted 28 March 2012)

ABSTRACT

One of the main concerns for pipeline on-bottom stability design is to properly predict ultimate soil resistance in severe ocean environments. A plane-strain finite element model is proposed to investigate the ultimate soil resistance to the partially-embedded pipeline under the action of ocean currents. Two typical end-constraints of the submarine pipelines are examined, i.e. freely-laid pipes and anti-rolling pipes. The proposed numerical model is verified with the existing mechanical-actuator experiments. The magnitude of lateral-soil-resistance coefficient for the examined anti-rolling pipes is much larger than that for the freely-laid pipes, indicating that the end-constraint condition significantly affects the lateral stability of the untrenched pipeline under ocean currents. The parametric study indicates that, the variation of lateral-soil-resistance coefficient with the dimensionless submerged weight of pipe is affected greatly by the angle of internal friction of soil, the pipe-soil friction coefficient, etc.

Key words: *submarine pipeline*; *on-bottom stability*; *ultimate soil resistance*; *ocean current*; *sandy seabed*

1. Introduction

The on-bottom stability of a submarine pipeline involves complex interactions between the wave/current, the untrenched pipeline and the neighboring soil. To avoid the occurrence of pipeline on-bottom (lateral) instability, i.e. the breakout of the pipe from its original site, the seabed must provide enough soil resistance to balance the hydrodynamic loads upon the untrenched pipeline. For pipeline geotechnical engineers, one of the main concerns for pipeline on-bottom stability design is to properly predict the ultimate soil resistance in the severe ocean environments, and to further determine the thickness of coating layers based on nominal pipe weight (Det Norske Veritas, 2007).

In the past few decades, the pipe-soil interactions have attracted much interest from pipeline researchers and designers. Numerous experimental studies on wave-induced pipe instability have been carried out with 1g mechanical actuators (Wagner *et al*., 1987; Palmer *et al*., 1988), with centrifugal pipe-soil interaction tests on calcareous sand (Zhang *et al*., 2002), and with flume hydrodynamic simulations (Gao *et al*., 2003; Teh *et al*., 2003). Several empirical “pipe-soil” or “wave-pipe-soil” interaction models were developed to improve the conventional Coulomb friction theory. Wagner *et al*. (1987) proposed a pipe-soil interaction model, in which both the pipe-soil friction component and soil passive-pressure component are included in the total lateral resistance to the untrenched pipe. Zhang *et al*.

* The project was financially supported by the Knowledge Innovation Program of Chinese Academy of Sciences (Grant No. KJCX2-YW-L07).
1 Corresponding author. E-mail: fpgao@imech.ac.cn

(2002) conducted a series of centrifugal tests and established a non-associated bounding surface model to simulate the response of a pipeline embedded in sandy soil under combined vertical and horizontal monotonic loading. Based on test results of a U-shaped oscillatory flow water tunnel, Gao *et al*. (2003) proposed the new criteria for pipeline on-bottom stability on the sand-bed. Some reviews on pipeline geotechnics and pipe-soil interactions have been made recently by Cathie *et al*, (2005), White and Randolph (2007), etc. Note that the aforementioned studies mainly focused on the pipeline on-bottom stability subjected to ocean waves.

As the oil and gas exploitation moving into deeper waters, ocean current becomes the prevailing hydrodynamic load for on-bottom stability of submarine pipelines. Although the pipe on-bottom stability in currents seems less complicated than in waves, till now, the underlying physical mechanism has not been well revealed (Gao *et al*., 2007).

To further explore the mechanism of pipeline on-bottom stability in ocean currents, a plane-strain finite element model is proposed and verified with the mechanical-actuator tests. The ultimate lateral soil resistance to the untrenched pipes with two kinds of constraint conditions, i.e. freely-laid pipes and anti-rolling pipes, is investigated numerically.

2. Plane-Strain FE Model for Pipe-Soil Interaction

2.1 Finite Element Mesh and Boundary Conditions

As the length of a submarine pipeline is much larger than its diameter, the pipeline lateral stability can be treated as a plane-strain problem. A plane-strain finite element model is proposed for simulating the breakout of the pipeline from its original site. The typical finite element mesh is illustrated in Fig. 1.

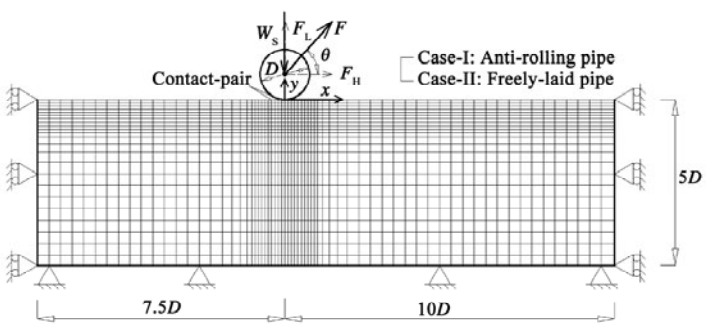

Fig. 1. Typical plane-strain finite element mesh (not in scale) and boundary conditions for pipe lateral stability analyses.

The boundary conditions are set as follows: (1) at the left and right boundary, no displacement in the x direction takes place; (2) the bottom boundary is fixed, i.e. the displacement and rotation are not permitted; (3) at the pipe-soil interface, the contact-pair algorithm provided in the ABAQUS software (Hibbitt, Karlsson and Sorensen Inc, 2006) is adopted to simulate the moving pipe along the deformable soil. The non-contact soil surface is treated as a free boundary. In the numerical modelling of the pipeline losing on-bottom stability, it is crucial to properly describe the contact conditions between the pipe and the neighbouring soil. The pipe-soil friction is defined by the Penalty Function

with the advantage that it guarantees the positive definiteness of sparse matrix in the calculation. In order to avoid large distortion of finite elements causing the calculation misconvergence, the self-adaptive mesh technology is employed.

To obtain high calculation efficiency, the finite element mesh gets more refined at closer proximity to the pipe. Based on the results of a series of trial calculations, the width of the numerical model is set as 17.5D and the depth as 5D, and the pipeline is located at $x = 7.5D$ (D is the pipeline diameter), as shown in Fig. 1.

2.2 End-Constraint and Simulation of Ocean Current Loading on the Pipeline

For a long-distance laid pipeline, the on-bottom stability of the pipeline at its separate sections is different. Owing to the constraints from risers and the pipeline own anti-torsion rigidity, the pipeline movement is neither purely parallel nor purely rotational. As such, the following two end-constraint conditions are taken into account in the present study. Case I: Anti-rolling pipe. The pipe's rolling is restricted, but the pipe can move freely in the horizontal and vertical directions; Case II: Freely-laid pipe. The pipe may rotate around its axis without any end constraint.

When a pipeline is laid on the seabed under the action of ocean currents, there exists a dynamic balance between the submerged weight of the pipe, the hydrodynamic forces (including the horizontal drag force F_{D} and the vertical lift force F_{L}), and the soil resistances. When the ultimate lateral soil resistance can not balance the horizontal drag force, the pipe would break out from its original site, i.e. the lateral instability occurs.

To efficiently simulate the ocean currents induced hydrodynamic loads upon a submarine pipeline is crucial for evaluating pipeline lateral on-bottom stability. According to Morison's equation, the horizontal and lift (vertical) components of the steady flow induced horizontal drag force and vertical lift force are respectively expressed as:

$$F_{\mathrm{D}} = \frac{1}{2} C_{\mathrm{D}} \rho_{\mathrm{w}} D U^2; \tag{1}$$

$$F_{\mathrm{L}} = \frac{1}{2} C_{\mathrm{L}} \rho_{\mathrm{w}} D U^2, \tag{2}$$

where C_{D} is the drag coefficient, C_{L} is the lift coefficient, ρ_{w} is the mass density of water, and U is the effective water particle velocity. The variations of the drag and lift coefficients, C_{D} and C_{L}, with the Reynolds number (Re) for various values of pipe surface roughness have been obtained by Jones (1978). The resultant hydrodynamics force upon the pipe is exerted obliquely upwards with the inclination angle:

$$\theta = \arctan\left(F_{\mathrm{L}}/F_{\mathrm{D}}\right) \approx \arctan\left(C_{\mathrm{L}}/C_{\mathrm{D}}\right). \tag{3}$$

As referring to the experimental results by Jones (1978), the inclination angle (θ) is approximately between $53° \sim 57°$. It is therefore reasonable to apply an inclined force in the θ direction to simulate the hydrodynamic loads on the pipe in the steady ocean currents.

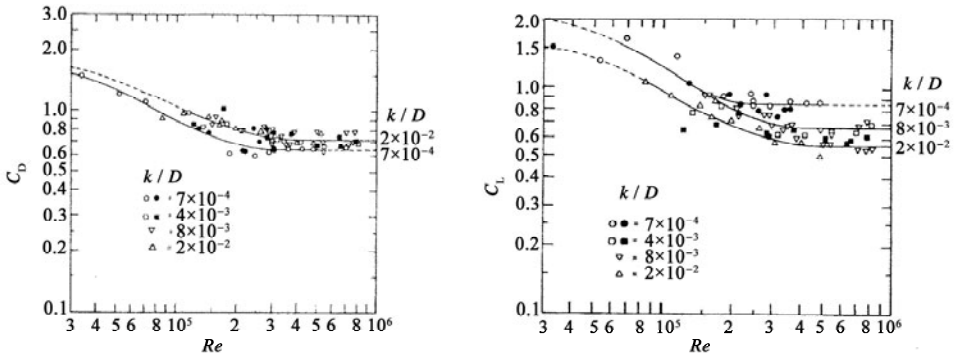

Fig. 2. Effective hydrodynamic coefficients for a pipe resting on the sea bottom recommended by Jones (1978).

2.3 Constitutive Model for Sandy Soil and Its Properties

The sandy soil under drained conditions can be essentially assumed to behave as an elastic $c-\phi$ material (Mohr-Coulomb or D-P material). The seabed soil is simulated with the well-known extended Drucker-Prager (D-P) elastoplasticity constitutive model. The yield criterion of the extended Drucker-Prager model is written as:

$$t - p\tan\beta - d = 0\,, \tag{4}$$

where t is the deviatoric stress defined as:

$$t = \frac{q}{2}\left[1+\frac{1}{K}-\left(1-\frac{1}{K}\right)\left(\frac{R}{q}\right)^3\right], \tag{5}$$

in which β is the slope of the linear yield surface in the p–t stress plane; p is the equivalent pressure stress; R is the third invariant of deviatoric stress; q is the Mises equivalent stress; d is the cohesion of the material; K is the ratio of the yield stress in triaxial tension to the yield stress in triaxial compression. The extended D-P model is preferable to reflect the granular-like property of frictional materials and exhibit pressure-dependent yield. The extended D-P model gives a good approximation to the Mohr-Coulomb model. The relationship of the parameters in the two constitutive models are as follows: $\tan\beta = \sqrt{3}\sin\phi$; $d = \sqrt{3}\cos\phi\cdot c$, where ϕ is the angle of internal friction of soil, and c is the cohesive strength of soil. The extended D-P model defines the yield surface as a circle in the deviatoric π plane while for the Mohr-Coulomb model it is a hexagon, which will benefit the convergence of the iterative algorithm.

In the simulations, the parameters of soil are chosen as follows: Young's modulus E = 0.18 MPa, Poisson's ratio $\nu = 0.32$, the cohesion $c = 0$, the buoyant unit weight of the soil $\gamma' = 9.3\times10^3$ N/m^3, and the values of the angle of internal friction of the soil (ϕ) are various for the parametric study in Section 4.1.

As aforementioned, the pipe is treated as a rigid cylinder with the outer diameter $D = 0.15$ m (same as the test pipes). The submerged weight of the pipe per meter (W_S) and the pipe-soil friction coefficient (μ) are various for the parametric studies in Section 4. Owing to that the stiffness of the

steel pipeline with concrete cover is normally larger than that of the soil, and the wall of the pipeline is regarded as a rigid cylinder in this finite element analysis.

3. Verification of the Proposed Numerical Model

To verify the proposed numerical model, an updated experimental facility by employing the mechanical-actuator simulation method has recently been designed and constructed (Gao *et al*., 2011). This facility mainly consists of a sand box with glass wall, a mechanical-actuator, and the measurement system, etc. In the sand box (2 m long, 0.5 m wide and 0.6 m deep), a saturated sand-bed with certain relative density can be prepared by employing the sand-raining technique. In the mechanical-actuator system, a stepper motor is capable of generating the inclined force onto the test pipe via a cable passing through a fixed pulley, for simulating steady currents induced drag force and lift force on the pipeline. Meanwhile, a lifter is used to adjust the inclination angle, which is maintained in the range of $53°\sim57°$ according to the above analyses.

Fig. 3(a) illustrates the typical development of lateral soil resistance and the corresponding vertical pipe-soil contact force for an anti-rolling pipe when losing lateral stability. With the increase of horizontal displacement (S_x) during the pipe losing lateral stability, the horizontal lateral soil resistance (F_{H}) increases gradually to its maximum value ($F_{\mathrm{u}} = 0.10$ kN/m) when the additional settlement is nearly fully developed according to the experimental observation. Meanwhile, the corresponding vertical pipe-soil contact force ($W_{\mathrm{S}} - F_{\mathrm{H}} \tan\theta$) decreases gradually to its minimum value (0.085 kN/m). The FEM numerical results match well with the test results. Fig. 3(b) shows the numerical results of the plastic deformation beneath the anti-rolling pipe while losing lateral stability. It is indicated that the shear band is distributed underneath the deformed soil layer; meanwhile, the soil just in front of the moving pipe upheaves obviously (see Fig. 3(b)).

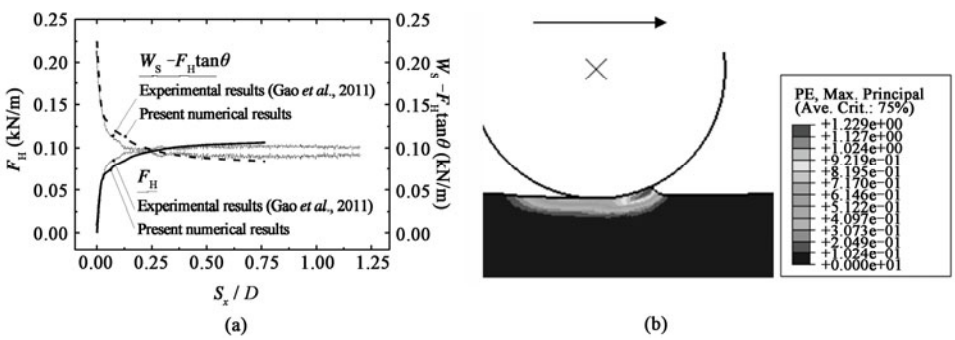

Fig. 3. (a) Development of the lateral soil resistance and the corresponding vertical pipe-soil contact force for an anti-rolling pipe when losing lateral stability: Comparison between numerical and experimental results; (b) Plastic deformation beneath the anti-rolling pipe while losing lateral stability ($D = 0.15$ m, $\mu = 0.7$, $W_{\mathrm{S}} = 0.225$ kN/m, and $\phi = 26.7°$).

The variation of ultimate lateral soil resistance (F_{u}) with the vertical pipe-soil contact force ($W_{\mathrm{S}} - F_{\mathrm{u}} \tan\theta$) is given in Fig. 4, indicating that the numerical and the experimental results are quite

comparable. The ultimate lateral soil resistance increases linearly with the vertical pipe-soil contact force. The proposed FEM model is capable of predicting the lateral resistance for the untrenched pipeline on-bottom instability.

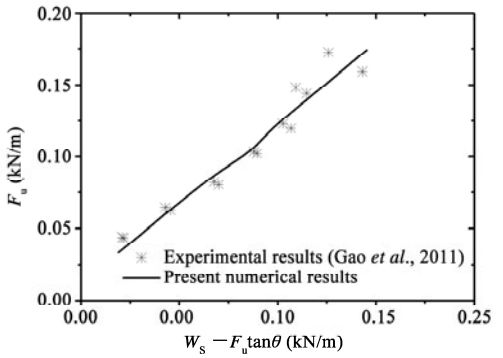

Fig. 4. Variation of ultimate lateral soil resistance with vertical pipe-soil contact force: Comparison between the numerical and the experimental results ($D = 0.15$ m , $\mu = 0.7$, and $\phi = 26.7°$).

4. Numerical Results and Analyses

In the process of a pipeline losing lateral stability under the action of ocean currents, the soil plastic deformation beneath the untrenched pipeline may be created due to the intensive pipe-soil interaction. Figs. 5(a) and 5(b) illustrate the plastic strain in the proximity of an anti-rolling pipeline and that of a freely-laid pipeline, respectively. It is indicated that, the end-constraint condition has much influence on the distribution of the plastic strain zone in the soil. For the anti-rolling pipeline, an obvious shear strain band may be formed in the underlying soil layer, and the soil upheave occurs in front of the moving pipeline (see Fig. 5(a)). Nevertheless, for the freely-laid pipeline, the smaller plastic-strain zone is created just underneath the rolling pipeline (see Fig. 5(b)).

As discussed above, many factors influencing the pipe-soil interaction could be incorporated in the proposed finite element model. In the following sections, the effects of soil internal friction angle and the pipe-soil friction coefficient on the on-bottom stability of the pipelines with two kinds of end-constraint will be further investigated numerically.

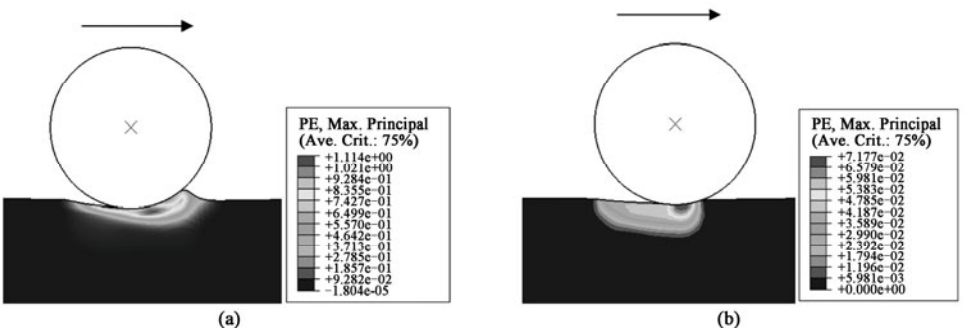

Fig. 5. Plastic deformation beneath the pipe while losing lateral stability: (a) Anti-rolling pipe; (b) Freely-laid pipe ($D = 0.15$ m , $W_S = 0.439$ kN/m , $\mu = 0.7$, and $\phi = 20°$).

4.1 Effects of the Angle of Internal Friction of Soil

For better understanding the pipe-soil interaction mechanism for on-bottom stability, a lateral-soil-resistance coefficient (η) is proposed, whose physical meaning is the ratio of the ultimate value of the horizontal lateral soil resistance to the corresponding vertical pipe-soil contact force, i.e.

$$\eta = \frac{F_u}{W_S - F_u \tan\theta}. \tag{6}$$

The commonly-used dimensionless submerged weight (G) of the pipe is

$$G = \frac{W_S}{\gamma' D^2}, \tag{7}$$

where γ' is the buoyant unit weight of the saturated sand.

Both the experimental and numerical results show that, in addition to the initial embedment due to the self-weight of the pipe in the process of losing lateral stability, some additional settlements may be developed while the horizontal lateral soil resistance increases gradually to its maximum value.

Figs. 6(a) and 6(b) give the variation of the maximum pipe settlement (e_m/D) with the dimensionless pipe's submerged weight (G) and that of the corresponding lateral soil resistance coefficient (η) with G for various values of the angle of internal friction of the soil for the case of anti-rolling pipeline with a given diameter ($D = 0.15$ m). The maximum pipeline settlements (e_m/D) in the process of pipeline losing stability increase approximately linearly with the value increase of G. For the same value of G, e_m/D increases with the decrease of the angle of internal friction of the soil, especially for the larger submerged weights of the pipe (see Fig. 6(a)). The lateral-soil-resistance coefficient (η) decreases gradually to a constant value with the increase of G. The effect of soil internal friction angle on η gets more significant with increasing submerged weight of the pipeline.

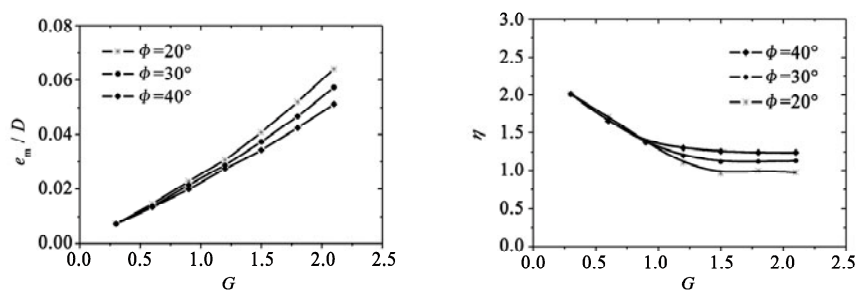

(a) e_m/D vs. G (b) η vs. G

Fig. 6. Lateral stability of anti-rolling pipes for various values of the angle of internal friction of soil ($D = 0.15$ m and $\mu = 0.7$).

Similarly, the variation of e_m/D with G and that of η with G for the case of freely-laid pipelines are given in Figs. 7(a) and 7(b). Compared with the case of anti-rolling pipelines (see Fig. 6), the relationships between e_m/D and G for the freely-laid pipes follow similar trends, but the maximum settlements are somewhat less in magnitude. Unlike the case of anti-rolling pipe, the effect

of ϕ on the variation of η with G for the freely-laid pipeline is different, i.e. η decreases with the increase of ϕ for a fixed value of G (e.g. G >1.0, see Fig. 7(b)). This may attribute to that the pipe settles more shallowly into the soil with the bigger angle of the internal friction, and that the freely-laid pipe tends to roll away from its original site. Note that the range of η for the examined anti-rolling pipes is between 1.0~2.0 (see Fig. 6(b)), but that for the freely-laid pipes only between 0.2~0.3 (see Fig. 7(b)). Therefore, the end-constraints have a significant influence on the lateral stability of the untrenched pipeline in ocean currents.

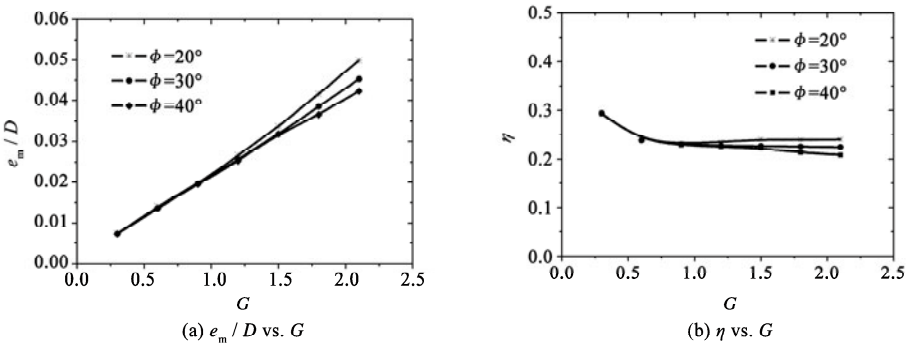

Fig. 7. Lateral stability of freely-laid pipes for various values of internal friction angle (D = 0.15 m and μ = 0.7).

4.2 Effects of Pipe-Soil Friction Coefficient

The submarine pipeline is usually constructed with a concrete cover. As imagined, the pipe-soil friction coefficient may affect the lateral stability of the pipeline.

Figs. 8 (a) and (b) give the variation of e_m/D with G and that of η with G for various values of pipe-soil friction coefficient (μ), respectively. For the case of anti-rolling pipes, the increase of μ brings an increase of the maximum settlement in the process of pipe losing lateral stability (see Fig. 8(a)). The effect of pipe-soil friction coefficient is more obvious for the smaller value of G. Its effect on the variation of η with G gets less with the decrease of μ (see Fig. 8(b)).

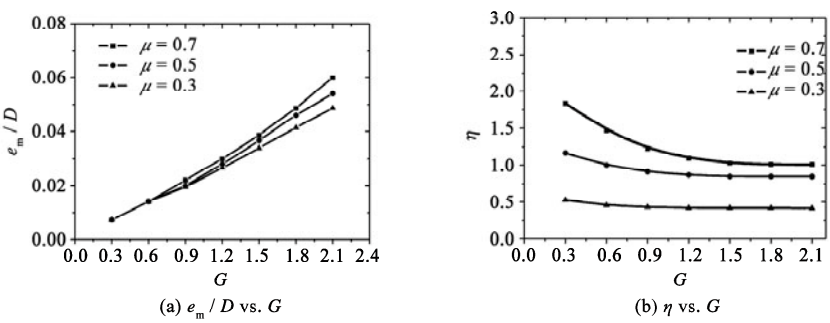

Fig. 8. Effects of the pipe-soil friction coefficients on the lateral stability of anti-rolling pipes (D = 0.15 m and ϕ = 26.7 °).

5. Concluding Remarks

As the offshore oil and gas exploitation moving into deeper waters, ocean current becomes the prevailing hydrodynamic load for on-bottom stability of submarine pipelines. In this paper, a finite element model is proposed and verified with the existing mechanical-actuator experiments. A parametric study is made to investigate the pipe-soil interaction mechanism for the current-induced pipeline lateral instability. The following conclusions can be drawn:

(1) The finite element model can effectively simulate the behavior of pipeline losing lateral stability in ocean currents under two end-constraint conditions, i.e. anti-rolling pipes and freely-laid pipes. The ultimate lateral soil resistance can be obtained from the load vs. displacement curve.

(2) A lateral-soil-resistance coefficient (η) is presented for better understanding pipe-soil interaction mechanism. The value of η decreases gradually to a constant with the increase of G. The magnitude of η for the examined anti-rolling pipes is much larger than that for the freely-laid pipes, indicating that the end-constraint condition affects significantly the lateral stability of the untrenched pipeline in ocean currents.

(3) For certain end constraint, either anti-rolling pipes or freely-laid pipes, the variation of η with G is affected by various parameters, including soil internal friction angle, pipe-soil friction coefficient, etc. The effect of pipe-soil friction coefficient is more obvious for the smaller value of G.

(4) When evaluating the capacity of lateral resistance, it would be beneficial to further examine and get correlation with the maximum pipeline penetration (including initial and additional settlement) and the development of the plastic-strain zone beneath the pipeline.

References

Cathie, D. N., Jaeck, C., Ballard, J. C. and Wintgens, J. F., 2005. Pipeline geotechnics: state-of-the-art, *Proceedings of Frontiers in Offshore Geotechnics*, *ISFOG 2005*, 95~114.

Det Norske Veritas, 2007. *On-Bottom Stability Design of Submarine Pipelines*, Recommended Practice, DNV-RP-F109.

Gao, F. P., Gu, X. Y. and Jeng, D. S., 2003. Physical modeling of untrenched submarine pipeline instability, *Ocean Eng*., **30**(10): 1283~1304.

Gao, F. P., Yan, S. M., Yang, B. and Wu, Y. X., 2007. Ocean currents-induced pipeline lateral stability on sandy seabed, *J. Eng. Mech*., ASCE, **133**(10): 1086~1092.

Gao, F. P., Yan, S. M., Yang, B. and Luo, C. C., 2011. Steady flow-induced instability of a partially embedded pipeline: Pipe–soil interaction mechanism, *Ocean Eng*., **38**(7): 934~942.

Hibbitt, Karlsson and Sorensen Inc, 2006. *ABAQUS Theory Manual*, Version 6.5-1.

Jones, W. T., 1978. On-bottom pipeline stability in steady water currents, *Journal of Petroleum Technology*, **30**(3): 475~484.

Palmer, A. C., Steenfelt, J. S., Steensen-Bach, J. O. and Jacobsen, V., 1988. Lateral resistance of marine pipelines on sand, *Proceedings of the 20th Annual Offshore Technology Conference*, OTC 5853, 399~408.

Teh, T. C., Palmer, A. C. and Damgaard, J. S., 2003. Experimental study of marine pipelines on unstable and liquefied seabed, *Coast. Eng*., **50**(1-2): 1~17.

Wagner, D. A., Murff, J. D., Brennodden, H. and Sveggen, O., 1987. Pipe-soil interaction model, *Proceedings of the 19th Annual Offshore Technology Conference*, OTC 5504, 181~190.

White, D. J. and Randolph, M. F., 2007. Seabed characterisation and models for pipeline-soil interaction, *Proceedings of the 17th International Offshore and Polar Engineering Conference*, Lisbon, 758~769.

Zhang, J. G., Stewart, D. P. and Randolph, M. F., 2002. Modeling of shallowly embedded offshore pipelines in calcareous sand, *Journal of Geotechnical and Geoenvironmental Engineering*, ASCE, **128**(5): 363~371.